View metadata, citation and similar papers at core.ac.uk
brought to you by CORE
provided by Digitale Bibliothek Thüringen

17th International Conference on the Application of Computer
Science and Mathematics in Architecture and Civil Engineering
K. Gürlebeck and C. Könke (eds.)
Weimar, Germany, 12–14 July 2006

AN IMPROVED COHESIVE CRACK MODEL FOR COMBINED CRACK OPENING AND SLIDING UNDER CYCLIC LOADING

T. Most, S. Eckardt, K. Schrader and T. Deckner

Institute of Structural Mechanics
Bauhaus-University Weimar, Germany
E-mails:thomas.most@uni-weimar.de
stefan.eckardt@uni-weimar.de
kai.schrader@uni-weimar.de
torsten.deckner@uni-weimar.de

Keywords: Cohesive crack model, mixed-mode cracking, dilatancy, cycling loading, plastic-damage formulation, parameter identification, neural networks

Abstract. *The modeling of crack propagation in plain and reinforced concrete structures is still a field for many researchers. If a macroscopic description of the cohesive cracking process of concrete is applied, generally the Fictitious Crack Model is utilized, where a force transmission over micro cracks is assumed. The cohesive forces are calculated in this model only from the normal stresses.*

Later an improved model was developed using a coupled relation between the normal and shear damage based on an elasto-plastic constitutive formulation, where the inelastic crack opening is represented by plastic strains. Thus this model is limited for applications with monotonic loading. In order to enable the application for cases with un- and reloading the existing model is extended here using a combined plastic-damage formulation, which enables the modeling of crack opening and crack closure.

Finally an investigation concerning the identification of the model parameters by means of neural networks is presented. In this analysis an inverse approximation of the model parameters is performed by using a given set of points of the load displacement curves as input values and the model parameters as output terms.

1 INTRODUCTION

The modeling of crack propagation in plain and reinforced concrete structures is still a field for many researchers. If a macroscopic description of the cohesive cracking process of concrete is applied, generally the Fictitious Crack Model is utilized [1], where a force transmission over micro cracks is assumed. In the most applications of this concept the cohesive model represents the relation between the normal crack opening and the normal stress, which is mostly defined as an exponential softening function, independently from the shear stresses in tangential direction. The cohesive forces are then calculated only from the normal stresses.

In [2] an improved model was developed using a coupled relation between the normal and shear damage based on an elasto-plastic constitutive formulation. This model is based on a hyperbolic yield surface depending on the normal and the shear stresses and on the tensile and shear strength. This model also represents the effect of shear traction induced crack opening. In [3] an algorithmic implementation of this model using an implicit return mapping algorithm was realized. In [4] and [5] this model has been applied within an automatic algorithm for the discrete simulation of mixed mode cracking in concrete.

Due to the elasto-plastic formulation, where the inelastic crack opening is represented by plastic strains, this model is limited for applications with monotonic loading. In order to enable the application for cases with un- and reloading the existing model is extended in this study using a combined plastic-damage formulation, which enables the modeling of crack opening and crack closure. Furthermore the corresponding algorithmic implementation using a return mapping approach is presented and the model is verified by means of several numerical examples.

Finally an investigation concerning the identification of the model parameters by means of neural networks is presented. In this analysis an inverse approximation of the model parameters is performed by using a given set of points of the load displacement curves as input values and the model parameters as output terms.

2 MECHANICAL MODEL

2.1 Elasto-plastic formulation

The degradation of the crack surface is described by [2] in terms of the classical plasticity theory, where the well-known continuum formulation is transferred into an interface formulation, where relative displacements $\mathbf{\Delta u}$ in the crack surface are used instead of strains. Based on a decomposition of $\mathbf{\Delta u}$ into an elastic part $\mathbf{\Delta u}^{el}$ and a plastic part $\mathbf{\Delta u}^{cr}$ in the following form

$$\mathbf{\Delta u} = \begin{bmatrix} \Delta u_N \\ \Delta u_{T1} \\ \Delta u_{T2} \end{bmatrix} = \mathbf{\Delta u}^{el} + \mathbf{\Delta u}^{cr} = \begin{bmatrix} \Delta u_N^{el} + \Delta u_N^{cr} \\ \Delta u_{T1}^{el} + \Delta u_{T1}^{cr} \\ \Delta u_{T2}^{el} + \Delta u_{T2}^{cr} \end{bmatrix}, \tag{1}$$

the stresses in the crack surface are defined as

$$\boldsymbol{\sigma} = \begin{bmatrix} \sigma_N \\ \sigma_{T1} \\ \sigma_{T2} \end{bmatrix} = \mathbf{C}\left(\mathbf{\Delta u} - \mathbf{\Delta u}^{cr}\right) = \begin{bmatrix} k_N & 0 & 0 \\ 0 & k_T & 0 \\ 0 & 0 & k_T \end{bmatrix} \begin{bmatrix} \Delta u_N - \Delta u_N^{cr} \\ \Delta u_{T1} - \Delta u_{T1}^{cr} \\ \Delta u_{T2} - \Delta u_{T2}^{cr} \end{bmatrix}, \tag{2}$$

where $\mathbf{C}$ is the elastic material stiffness matrix, which contains only decoupled terms, and Δu_N, Δu_{T1}, Δu_{T2} and σ_N, σ_{T1}, σ_{T2} are the relative displacements and the stresses in the normal and

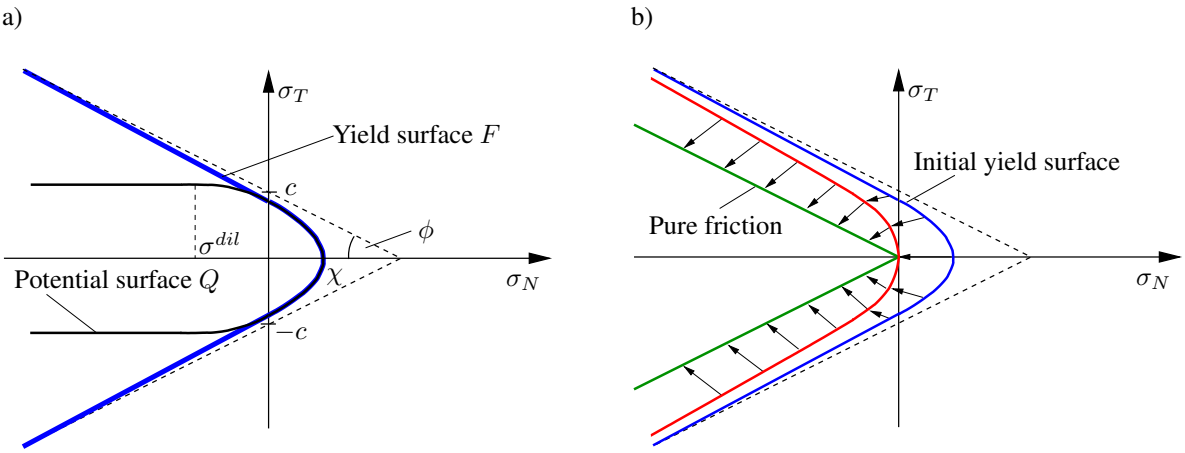

Figure 1: a) Hyperbolic yield surface and plastic potential, b) Development of yield surface

in two tangential directions, respectively. For the 3D case the tangential directions can be chosen arbitrary as long as they span a Cartesian coordinate system with the normal direction, which is defined by the crack surface. The elastic stiffness values k_N and k_T are numerical parameters for the activation of the normal and shear stresses without physical meaning.

The fracture process is described by a hyperbolic yield surface shown in Fig. 1a

$$F = \sigma_T^2 - (c - \sigma_N \tan\phi)^2 + (c - \chi \tan\phi)^2, \quad \sigma_T = \sqrt{\sigma_{T1}^2 + \sigma_{T2}^2}, \tag{3}$$

where $\tan\phi$ is the friction coefficient for Coulomb friction and c and χ are internal variables belonging to the actual shear and tensile strength, respectively. If the value of the yield criterion F is negative, the interface material is in an elastic state (initial or un-/reloading), and if F is equal to zero the material is in a plastic state, where the internal variables c and χ show a softening behavior with increasing plastic relative displacements $\mathbf{\Delta u}^{cr}$. In Fig. 1b the development from the initial yield surface to the state with completely destroyed interlocking of the crack surfaces is shown. This final state represents Coulomb's friction between two plain surfaces.

In [2] the softening behavior of χ and c is described in terms of the work W^{cr} spent on the fracture process during the formation of the crack. They are assumed to decrease from their initial values χ_0 and c_0, which are the initial tensile and shear strength taken as material parameters, to zero when $W^{cr} = G_f^I$ and $W^{cr} = G_f^{IIa}$, respectively. G_f^I is the Mode-I specific fracture energy, which is used in standard cohesive models, and G_f^{IIa} is the Mode-IIa specific fracture energy. The latter case is also called asymptotic Mode-II, where the crack opening due to dilatancy effects is avoided by very high compression forces. The variation of c and χ is defined by a scaling function ψ as

$$\begin{aligned} \chi &= \chi_0 - \chi_0\, \psi\left(\frac{W^{cr}}{G_f^I}, \alpha_\chi\right), \\ c &= c_0 - c_0\, \psi\left(\frac{W^{cr}}{G_f^{IIa}}, \alpha_c\right), \end{aligned} \tag{4}$$

with

$$\psi(\xi, \alpha) = \frac{\mathrm{e}^{-\alpha}\xi}{1 + (\mathrm{e}^{-\alpha} - 1)\,\xi}. \tag{5}$$

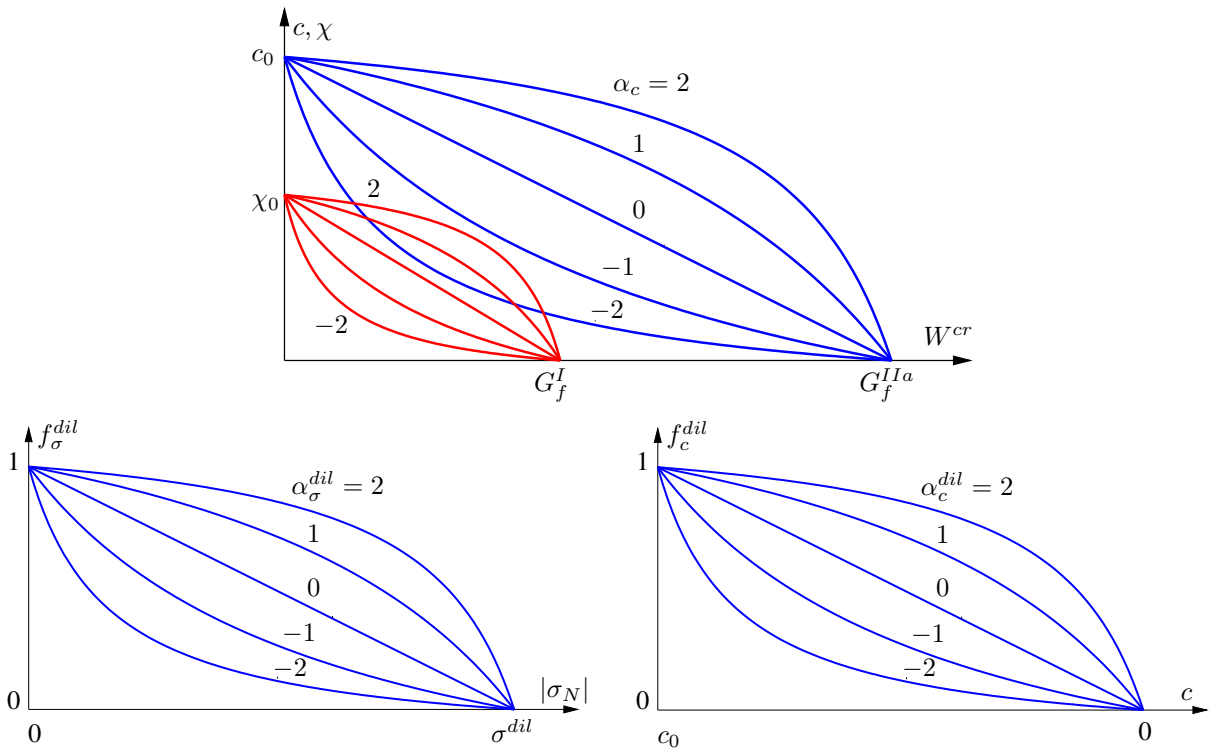

Figure 2: Functions for c, χ, f_σ^{dil} and f_c^{dil} depending on the shape parameters α_c, α_χ, α_σ^{dil} and α_c^{dil}

In Fig. 2 the softening curves for c and χ depending on W^{cr} are shown for different scaling parameters α_c and α_χ. Linear decreasing functions are obtained for $\alpha = 0$.

The change of the actual work W^{cr} is defined in [2] as

$$dW^{cr} = \begin{cases} \sigma_N du_N^{cr} + \sigma_{T1} du_{T1}^{cr} + \sigma_{T2} du_{T2}^{cr} & \sigma_N \geq 0 \\ (\sigma_{T1} du_{T1}^{cr} + \sigma_{T2} du_{T2}^{cr}) \left(1 - \left|\dfrac{\sigma_N \tan\phi}{\sigma_T}\right|\right) & \sigma_N < 0 \end{cases} \tag{6}$$

which implies, that in tension all dissipated work goes into the fracture process, while in compression only the shear work by subtracting the basic friction is considered.

The evolution of the plastic deformations is defined in classical plasticity theory by the plastic multiplier γ and by the flow direction, which is assumed to be perpendicular to the plastic potential surface Q. This leads to the well-known flow rule

$$d\mathbf{\Delta u}^{cr} = d\gamma \frac{\partial Q}{\partial \boldsymbol{\sigma}}. \tag{7}$$

In this model this potential surface is taken as the yield surface by introducing following two modifications: Initially the potential surface coincides with the yield surface in tension. For compression the dilatancy vanishes for a compressive stress higher than the dilatancy stress σ^{dil}, which is introduced as material parameter. Furthermore the amount of dilatancy has to decrease with increasing degradation of the crack surface. It vanishes completely for the pure friction state with $c = 0$. This leads to the following expressions for the derivatives of the plastic potential, which describe the yield direction

$$\frac{\partial Q}{\partial \sigma_N} = 2\tan\phi(c - \sigma_N \tan\phi) f_\sigma^{dil} f_c^{dil}, \quad \frac{\partial Q}{\partial \sigma_{T1}} = 2\sigma_{T1}, \quad \frac{\partial Q}{\partial \sigma_{T2}} = 2\sigma_{T2}, \tag{8}$$

where f_σ^{dil} and f_c^{dil} are the factors introduced to represent the two mentioned effects. These factors are defined using the scaling function in Eq. (5) as follows

$$
\begin{aligned}
f_\sigma^{dil} &= 1 - \psi\left(\frac{|\sigma_N|}{\sigma^{dil}}, \alpha_\sigma^{dil}\right), \\
f_c^{dil} &= 1 - \psi\left(\frac{c_0 - c}{c_0}, \alpha_c^{dil}\right).
\end{aligned}
\tag{9}
$$

The development of the factors f_σ^{dil} and f_c^{dil} is shown in Fig. 2 for different scaling parameters. The plastic potential is shown in Fig. 1a together with the yield surface for an initial material state. Altogether the presented model has twelve parameters, the elastic stiffnesses k_N and k_T, the initial tensile and shear strength χ_0 and c_0, the Mode-I and Mode-IIa specific fracture energy G_f^I and G_f^{IIa}, the friction coefficient tanϕ, the dilatancy stress σ^{dil} and four shape parameters, α_χ, α_c, α_σ^{dil} and α_c^{dil}, where the elastic stiffnesses are pure numerical parameters, which have to be taken as large as possible without causing numerical problems.

In this work the implementation of the presented model clarified a significant problem of the formulation, which limits the application to very small incremental steps. This problem is caused by the quadratic formulation of the yield surface in Eq. (3) concerning σ_N, which has two independent functions fulfilling $F = 0$. This is shown in Fig. 10. If the elastic predictor in the stress update procedure is too large, caused by large increments or high elastic stiffnesses, the iteration converges to the second zero line, which has no physical meaning. In the worst case elastic behavior is indicated if the elastic predictor is in the second domain with $F < 0$.

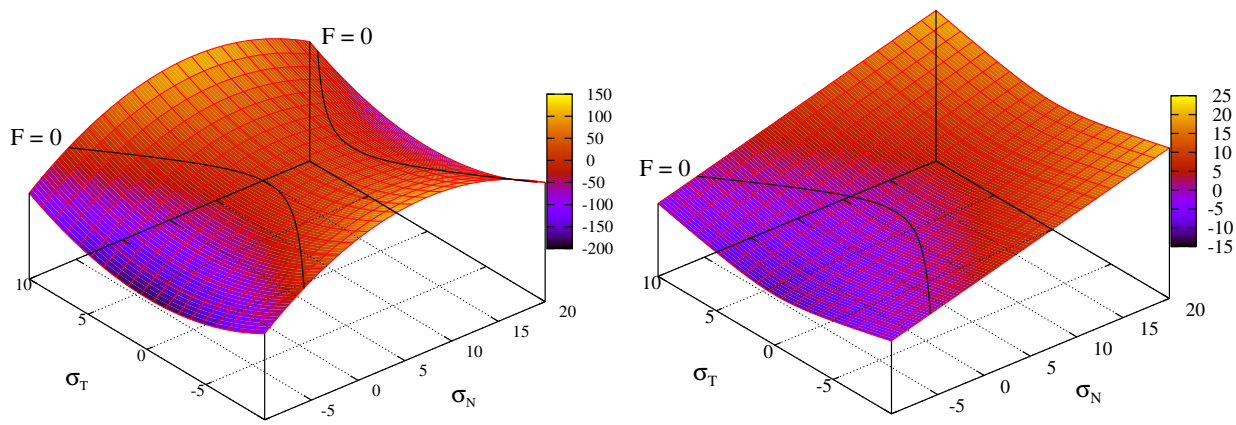

Figure 3: Original yield surface with two functions for $F = 0$ and modified surface with only one zero line

This problem is solved here, by transforming the original surface with quadratic terms to the following formulation

$$
F_{mod} = \sqrt{\sigma_T^2 + (c - \chi \tan\phi)^2} - c + \sigma_N \tan\phi, \tag{10}
$$

where no quadratic term concerning σ_N is included. Fig. 10 indicates, that the modified surface has only one function with $F = 0$, which coincides exactly with the first function of the original surface. The derivatives of the modified yield function lead to the following formulation of the

yield direction

$$\frac{\partial Q}{\partial \sigma_N} = \tan\phi f_\sigma^{dil} f_c^{dil}, \quad \frac{\partial Q}{\partial \sigma_{T1}} = \frac{\sigma_{T1}}{\sqrt{\sigma_T^2 + (c - \chi \tan\phi)^2}}, \quad \frac{\partial Q}{\partial \sigma_{T2}} = \frac{\sigma_{T2}}{\sqrt{\sigma_T^2 + (c - \chi \tan\phi)^2}}. \tag{11}$$

Due to the formulation of the softening function of c and χ in terms of the work W^{cr} and the scaling function $\psi(\xi, \alpha)$, the direct fitting of experimental curves, e.g. from uniaxial tension tests, is not possible. For linear or piecewise linear uniaxial softening curves, the function of c

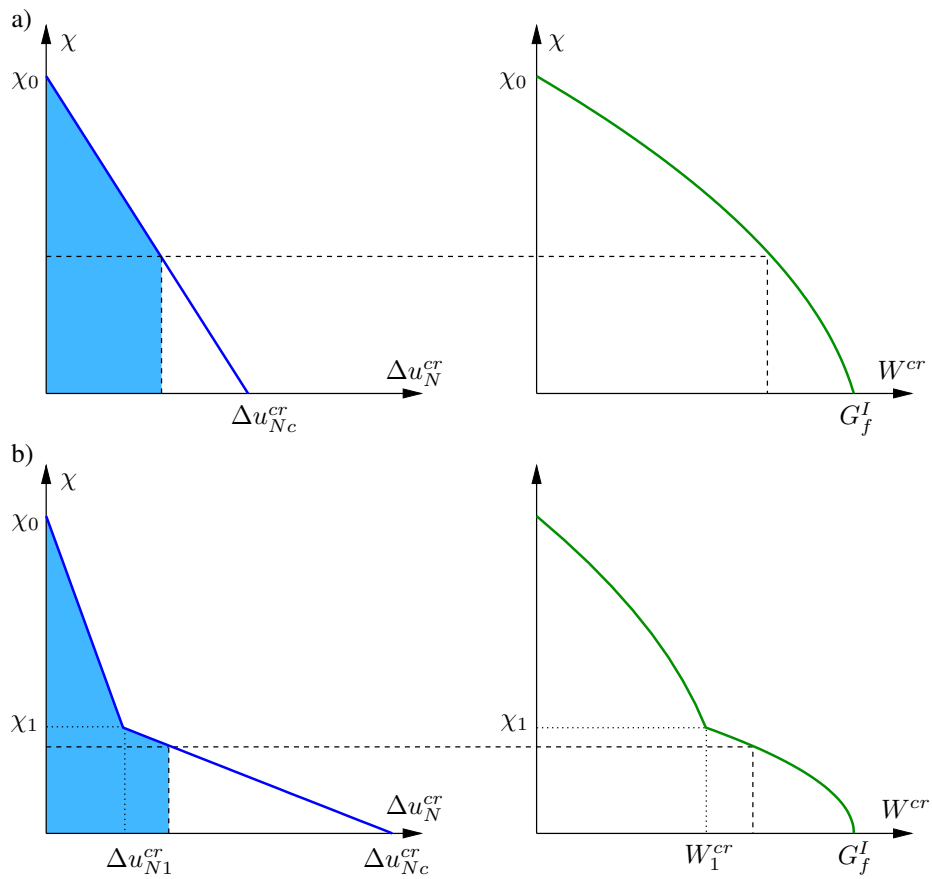

Figure 4: a) Linear and b) bilinear softening curves χ vs. Δu_N^{cr} and corresponding functions in terms of W^{cr}

and χ in terms of W^{cr} can be derived analytically. This enables an easy fitting of experimental data, e.g. using a bilinear approximation. For linear softening the function of χ in terms of W^{cr} reads

$$\chi^{linear}(W^{cr}) = \begin{cases} \chi_0 \sqrt{1 - \dfrac{W^{cr}}{G_f^I}} & W^{cr} \leq G_f^I \\ 0 & W^{cr} > G_f^I \end{cases} \tag{12}$$

which can be used analogous for c. For the general bilinear case, shown in Fig. 4, the following

softening function of χ in terms of Δu_N^{cr} can be formulated

$$\chi^{bilinear}(\Delta u_N^{cr}) = \begin{cases} \chi_0 - \dfrac{\chi_0 - \chi_1}{\Delta u_{N1}^{cr}} \Delta u_N^{cr} & \Delta u_N^{cr} \leq \Delta u_{N1}^{cr} \\ \chi_1 \dfrac{\Delta u_{Nc}^{cr} - \Delta u_N^{cr}}{\Delta u_{Nc}^{cr} - \Delta u_{N1}^{cr}} & \Delta u_{N1}^{cr} < \Delta u_N^{cr} \leq \Delta u_{Nc}^{cr} \\ 0 & \Delta u_N^{cr} > \Delta u_{Nc}^{cr} \end{cases} \tag{13}$$

which leads to

$$\chi^{bilinear}(W^{cr}) = \begin{cases} \chi_0 \sqrt{1 - 2W^{cr} \dfrac{\chi_0 - \chi_1}{\Delta u_{N1}^{cr} \chi_0^2}} & W^{cr} \leq W_1^{cr} \\ \chi_1 \sqrt{1 - \dfrac{2}{\chi_1} \dfrac{W^{cr} - W_1^{cr}}{\Delta u_{Nc}^{cr} - \Delta u_{N1}^{cr}}} & W_1^{cr} < W^{cr} \leq G_f^I \\ 0 & W^{cr} > G_f^I \end{cases} \tag{14}$$

with

$$W_1^{cr} = \frac{1}{2} \chi_1 (\Delta u_{Nc}^{cr} - \Delta u_{N1}^{cr}). \tag{15}$$

A detailed derivation of the formulation for the linear and the bilinear case can be found in [4].

2.2 Extension for cycling loading

In this section we present the extension of the original elasto-plastic model for cyclic loading. This is realized in this paper by using a plastic-damage formulation only in normal direction, where the total crack opening Δu_N is decomposed into an elastic part Δu_N^{el} and an inelastic part Δu_N^{cr}, whereby Δu_N^{cr} contains the plastic deformation Δu_N^{pl} and the deformation due to damage Δu_N^D. This assumptions leads to the following equation

$$\begin{aligned} \Delta u_N &= \Delta u_N^{el} + \Delta u_N^{cr}, \\ &= \Delta u_N^{el} + \Delta u_N^D + \Delta u_N^{pl}. \end{aligned} \tag{16}$$

The relation for the normal stress reads in general form

$$\sigma_N = k_N \left(\Delta u_N - \Delta u_N^{cr} \right), \tag{17}$$

which is specified as

$$\sigma_N = \begin{cases} (1 - \omega)\, k_N (\Delta u_N - \Delta u_N^{pl}) & \Delta u_N - \Delta u_N^{pl} > 0 \\ k_N (\Delta u_N - \Delta u_N^{pl}) & \Delta u_N - \Delta u_N^{pl} \leq 0 \end{cases} \tag{18}$$

where ω is a scalar variable describing the damage evolution, which is zero for the intact material and one for full damage without further normal stress transmission. In Eq. (18) it is assumed, that for negative normal stresses, which is equivalent to the contact case, the full elastic modulus k_N is used as shown in Fig. 5. For this case the deformation due to damage is zero. By considering this and by substituting Eq. (17) in the first part of Eq. (18) we get the following

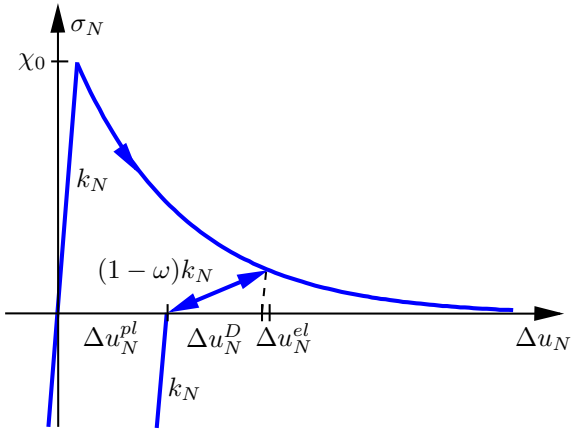

Figure 5: Damage evolution in normal direction

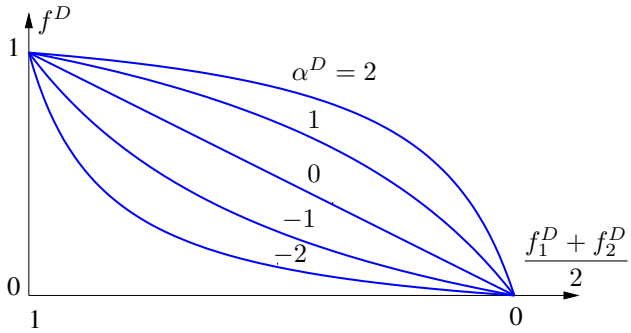

Figure 6: Scaling for the damage evolution factor

simple relation for the actual damage deformation Δu_N^D

$$\Delta u_N^D = \begin{cases} \omega\left(\Delta u_N - \Delta u_N^{pl}\right) & \Delta u_N - \Delta u_N^{pl} > 0 \\ 0 & \Delta u_N - \Delta u_N^{pl} \leq 0 \end{cases} \tag{19}$$

In this paper it is assumed, that the damage evolution for the pure crack opening case is defined by a parameter b which denotes the proportion of damage and plastic deformations. The flow rule for the plastic and damage displacements reads

$$\begin{aligned} d\Delta u_N^{pl} &= \quad (1 - bf^D)\, d\gamma \frac{\partial Q}{\partial \boldsymbol{\sigma}}, \\ d\Delta u_N^D &= \qquad bf^D\, d\gamma \frac{\partial Q}{\partial \boldsymbol{\sigma}}. \end{aligned} \tag{20}$$

If $b = 0$ no damage occurs and the model represents the pure elasto-plastic formulation. In this model it is assumed, that damage evolution is caused only by crack opening due to tensile loading in normal direction. For pure crack opening due to crack sliding without or with negative normal loading no damage evolution is allowed. These assumptions are included in the model by defining a scaling function f^D, which depends on the actual stress case

$$\begin{aligned} f^D &= 1 & \sigma_T &= 0, \sigma_N > 0, \\ 0 < f^D &< 1 & \sigma_T &> 0, \sigma_N > 0, \\ f^D &= 0 & \sigma_N &\leq 0. \end{aligned} \tag{21}$$

In order to define a suitable function f^D the two cases, namely $\sigma_T = 0$ and $\sigma_N = 0$ are used as the bounds for f^D. By using Eq. (10) we obtain the following stress states for these cases

$$\begin{aligned} f^D = 0: &\quad \sigma_N = 0 & \sigma_T &= \sqrt{2c\tan\phi - \tan^2\phi\chi^2}, \\ f^D = 1: &\quad \sigma_N = \chi & \sigma_T &= 0. \end{aligned} \tag{22}$$

Two scaling functions depending on the actual values of σ_T and σ_N are defined based on Eq. (22)

$$\begin{aligned} f_1^D &= 1 - \frac{\sigma_T}{\sqrt{2c\tan\phi - \tan^2\phi\chi^2}}, \\ f_2^D &= \frac{\sigma_N}{\chi}. \end{aligned} \tag{23}$$

In order to consider both functions and by introducing a shape parameter α^D and an exponent γ for a flexible shape of f^D, we define the following final formulation

$$f^D = \left[1 - \psi\left(1 - \frac{f_1^D + f_2^D}{2}, \alpha^D\right)\right]^\gamma. \tag{24}$$

In Fig. 6 the function f^D is shown for $\gamma = 1$ and different shape parameters.

2.3 Algorithmic implementation

2.3.1 Closest Point Projection Algorithm

In this section the adaptation of the General Closest Point Projection algorithm [6] for the presented cohesive crack model is derived. As unknown variables for the iteration the inelastic deformations $\mathbf{\Delta u}^{cr}$ and the dissipated fracture work W^{cr} are defined. The algorithm is based on the following incremental representation

$$\begin{aligned} \mathbf{\Delta u}_{n+1}^{cr} &= \mathbf{\Delta u}_n^{cr} + \delta \mathbf{\Delta u}_{n+1}^{cr}, \\ W_{n+1}^{cr} &= W_n^{cr} + \delta W_{n+1}^{cr}, \end{aligned} \tag{25}$$

where n defines the previous load step, where all unknown have been determined, and $n+1$ is the new load step, for which the implicit iteration has to calculate the required terms.

The increments of the inelastic displacement differences can be formulated by means of the flow direction, specified by the derivatives of the plastic potential, and the plastic multiplier γ

$$\delta \mathbf{\Delta u}_{n+1}^{cr} = \delta\gamma_{n+1} \frac{\partial Q_{n+1}}{\partial \boldsymbol{\sigma}}. \tag{26}$$

The evolution of W^{cr} defined in Eq. (6) can be written in incremental form as

$$\delta W_{n+1}^{cr} = \delta\gamma_{n+1} \frac{\partial \tilde{Q}_{n+1}}{\partial W^{cr}} \tag{27}$$

with

$$\frac{\partial \tilde{Q}}{\partial W^{cr}} = \begin{cases} \sigma_N \dfrac{\partial Q}{\partial \sigma_N} + \sigma_{T1} \dfrac{\partial Q}{\partial \sigma_{T1}} + \sigma_{T2} \dfrac{\partial Q}{\partial \sigma_{T2}} & \sigma_N \geq 0 \\ \left(\sigma_{T1} \dfrac{\partial Q}{\partial \sigma_{T1}} + \sigma_{T2} \dfrac{\partial Q}{\partial \sigma_{T2}}\right)\left(1 - \left|\dfrac{\sigma_N \tan\phi}{\sigma_T}\right|\right) & \sigma_N < 0 \end{cases} \tag{28}$$

The global residues can be defined as

$$\begin{aligned} \mathbf{R}_{n+1}^{\mathbf{\Delta u}^{cr}} &= -\mathbf{\Delta u}_{n+1}^{cr} + \mathbf{\Delta u}_n^{cr} + \delta\gamma_{n+1} \frac{\partial Q_{n+1}}{\partial \boldsymbol{\sigma}} &= \mathbf{0}, \\ R_{n+1}^{W^{cr}} &= -W_{n+1}^{cr} + W_n^{cr} + \delta\gamma_{n+1} \frac{\partial \tilde{Q}_{n+1}}{\partial W^{cr}} &= 0, \end{aligned} \tag{29}$$

and the yield criterion is given as

$$F_{n+1} = F(\boldsymbol{\sigma}_{n+1}, W_{n+1}^{cr}) = 0, \tag{30}$$

with

$$\boldsymbol{\sigma}_{n+1} = \mathbf{C}\left[\mathbf{\Delta u}_{n+1} - \mathbf{\Delta u}_{n+1}^{cr}\right]. \tag{31}$$

During the local iteration $\mathbf{\Delta u}_{n+1}$ remains constant, thus in the k-th iteration step the following relation is valid

$$\delta \mathbf{\Delta u}_{n+1}^{cr(k)} = -\mathbf{C}^{-1} \delta \boldsymbol{\sigma}_{n+1}^{(k)}. \tag{32}$$

This can be used to linearize Eq. (29)

$$\begin{aligned} &\mathbf{R}_{n+1}^{\mathbf{\Delta u}^{cr}(k)} - \delta \mathbf{\Delta u}_{n+1}^{cr(k)} + \delta^2 \gamma_{n+1}^{(k)} \frac{\partial Q_{n+1}^{(k)}}{\partial \boldsymbol{\sigma}} + \delta \gamma_{n+1}^{(k)} \frac{\partial^2 Q_{n+1}^{(k)}}{(\partial \boldsymbol{\sigma})^2} \delta \boldsymbol{\sigma}_{n+1}^{(k)} + \delta \gamma_{n+1}^{(k)} \frac{\partial^2 Q_{n+1}^{(k)}}{\partial \boldsymbol{\sigma} \partial W^{cr}} \delta W_{n+1}^{cr(k)} = \mathbf{0}, \\ &R_{n+1}^{W^{cr}(k)} - \delta W_{n+1}^{cr(k)} + \delta^2 \gamma_{n+1}^{(k)} \frac{\partial \tilde{Q}_{n+1}^{(k)}}{\partial W^{cr}} + \delta \gamma_{n+1}^{(k)} \left[\frac{\partial^2 \tilde{Q}_{n+1}^{(k)}}{\partial W^{cr} \partial \boldsymbol{\sigma}} \right]^T \delta \boldsymbol{\sigma}_{n+1}^{(k)} + \delta \gamma_{n+1}^{(k)} \frac{\partial^2 \tilde{Q}_{n+1}^{(k)}}{(\partial W^{cr})^2} \delta W_{n+1}^{cr(k)} = 0. \end{aligned} \tag{33}$$

In matrix-vector notation we can write

$$\mathbf{R}_{n+1}^{(k)} + \left[\mathbf{\Xi}_{n+1}^{(k)} \right]^{-1} \delta \mathbf{v}_{n+1}^{(k)} + \delta^2 \gamma_{n+1}^{(k)} \frac{\partial Q_{n+1}^{(k)}}{\partial \mathbf{v}} = \mathbf{0}, \tag{34}$$

with

$$\mathbf{R}_{n+1}^{(k)} = \begin{bmatrix} \mathbf{R}_{n+1}^{\mathbf{\Delta u}^{cr}(k)} \\ R_{n+1}^{W^{cr}(k)} \end{bmatrix}, \quad \delta \mathbf{v}_{n+1}^{(k)} = \begin{bmatrix} \delta \boldsymbol{\sigma}_{n+1}^{(k)} \\ \delta W_{n+1}^{cr(k)} \end{bmatrix}, \quad \frac{\partial Q_{n+1}^{(k)}}{\partial \mathbf{v}} = \begin{bmatrix} \dfrac{\partial Q_{n+1}^{(k)}}{\partial \boldsymbol{\sigma}} \\ \dfrac{\partial \tilde{Q}_{n+1}^{(k)}}{\partial W^{cr}} \end{bmatrix}, \tag{35}$$

where the Hessian matrix is given as

$$\mathbf{\Xi}_{n+1}^{(k)} = \begin{bmatrix} \mathbf{C}^{-1} + \delta \gamma_{n+1}^{(k)} \dfrac{\partial^2 Q_{n+1}^{(k)}}{(\partial \boldsymbol{\sigma})^2} & \delta \gamma_{n+1}^{(k)} \dfrac{\partial^2 Q_{n+1}^{(k)}}{\partial \boldsymbol{\sigma} \partial W^{cr}} \\ \delta \gamma_{n+1}^{(k)} \left[\dfrac{\partial^2 \tilde{Q}_{n+1}^{(k)}}{\partial W^{cr} \partial \boldsymbol{\sigma}} \right]^T & -1 + \delta \gamma_{n+1}^{(k)} \dfrac{\partial^2 \tilde{Q}_{n+1}^{(k)}}{(\partial W^{cr})^2} \end{bmatrix}^{-1}. \tag{36}$$

Linearizing Eq. (30) yields

$$F_{n+1}^{(k)} + \left[\frac{\partial F_{n+1}^{(k)}}{\partial \mathbf{v}} \right]^T \delta \mathbf{v}_{n+1}^{(k)} = 0, \quad \frac{\partial F_{n+1}^{(k)}}{\partial \mathbf{v}} = \begin{bmatrix} \dfrac{\partial F_{n+1}^{(k)}}{\partial \boldsymbol{\sigma}} \\ \dfrac{\partial F_{n+1}^{(k)}}{\partial W^{cr}} \end{bmatrix}. \tag{37}$$

Substitution of Eq. (34) in Eq. (37) reads

$$F_{n+1}^{(k)} + \left[\frac{\partial F_{n+1}^{(k)}}{\partial \mathbf{v}} \right]^T \mathbf{\Xi}_{n+1}^{(k)} \left[-\mathbf{R}_{n+1}^{(k)} - \delta^2 \gamma_{n+1}^{(k)} \frac{\partial Q_{n+1}^{(k)}}{\partial \mathbf{v}} \right] = 0. \tag{38}$$

Solving Eq. (38) with respect to $\delta^2 \gamma_{n+1}^{(k)}$ leads to the following relation

$$\delta^2 \gamma_{n+1}^{(k)} = \frac{F_{n+1}^{(k)} - \left[\dfrac{\partial F_{n+1}^{(k)}}{\partial \mathbf{v}} \right]^T \mathbf{\Xi}_{n+1}^{(k)} \mathbf{R}_{n+1}^{(k)}}{\left[\dfrac{\partial F_{n+1}^{(k)}}{\partial \mathbf{v}} \right]^T \mathbf{\Xi}_{n+1}^{(k)} \dfrac{\partial Q_{n+1}^{(k)}}{\partial \mathbf{v}}}. \tag{39}$$

The update for the iteration variables can be obtained from

$$\delta \mathbf{v}_{n+1}^{(k)} = -\boldsymbol{\Xi}_{n+1}^{(k)} \left[\mathbf{R}_{n+1}^{(k)} + \delta^2 \gamma_{n+1}^{(k)} \frac{\partial Q_{n+1}^{(k)}}{\partial \mathbf{v}} \right] \tag{40}$$

as follows

$$\begin{bmatrix} \delta \boldsymbol{\Delta} \mathbf{u}_{n+1}^{cr(k)} \\ \delta W_{n+1}^{cr(k)} \end{bmatrix} = \begin{bmatrix} \mathbf{C}^{-1} & \mathbf{0} \\ \mathbf{0} & -1 \end{bmatrix} \Xi_{n+1}^{(k)} \left[\mathbf{R}_{n+1}^{(k)} + \delta^2 \gamma_{n+1}^{(k)} \frac{\partial Q_{n+1}^{(k)}}{\partial \mathbf{v}} \right]. \tag{41}$$

Altogether we can formulate the algorithm, which is given in the Table 1 and Table 2.

2.3.2 Consistent algorithmic modulus

By differentiating the elastic-strain relationship in Eq. (31) and the algorithmic flow rule in Eq. (29) we obtain

$$d\boldsymbol{\sigma}_{n+1} = \mathbf{C} \left[d\boldsymbol{\Delta} \mathbf{u}_{n+1} - d\boldsymbol{\Delta} \mathbf{u}_{n+1}^{cr} \right] \tag{42}$$

and

$$\begin{aligned} d\boldsymbol{\Delta} \mathbf{u}_{n+1}^{cr} &= d\delta\gamma_{n+1} \frac{\partial Q_{n+1}}{\partial \boldsymbol{\sigma}} + \delta\gamma_{n+1} \frac{\partial^2 Q_{n+1}}{(\partial \boldsymbol{\sigma})^2} d\boldsymbol{\sigma}_{n+1} + \delta\gamma_{n+1} \frac{\partial^2 Q_{n+1}}{\partial \boldsymbol{\sigma} \partial W^{cr}} dW_{n+1}^{cr}, \\ dW_{n+1}^{cr} &= d\delta\gamma_{n+1} \frac{\partial \tilde{Q}_{n+1}}{\partial W^{cr}} + \delta\gamma_{n+1} \left[\frac{\partial^2 \tilde{Q}_{n+1}}{\partial W^{cr} \partial \boldsymbol{\sigma}} \right]^T d\boldsymbol{\sigma}_{n+1} + \delta\gamma_{n+1} \frac{\partial^2 \tilde{Q}_{n+1}}{(\partial W^{cr})^2} dW_{n+1}^{cr}. \end{aligned} \tag{43}$$

From the second part in Eq. (43) we can write

$$dW_{n+1}^{cr} = A \left[d\delta\gamma_{n+1} \frac{\partial \tilde{Q}_{n+1}}{\partial W^{cr}} + \delta\gamma_{n+1} \left[\frac{\partial^2 \tilde{Q}_{n+1}}{\partial W^{cr} \partial \boldsymbol{\sigma}} \right]^T d\boldsymbol{\sigma}_{n+1} \right], \tag{44}$$

with

$$A^{-1} = \left[1 - \delta\gamma_{n+1} \frac{\partial^2 \tilde{Q}_{n+1}}{(\partial W^{cr})^2} \right]. \tag{45}$$

By substituting Eq. (42) in the first part of Eq. (43) and by considering Eq. (44) we obtain

$$d\boldsymbol{\sigma}_{n+1} = \mathbf{B} \left[d\boldsymbol{\Delta} \mathbf{u}_{n+1} - d\delta\gamma_{n+1} \mathbf{D} \right], \tag{46}$$

with

$$\begin{aligned} \mathbf{B}^{-1} &= \mathbf{C}^{-1} + \delta\gamma_{n+1} \frac{\partial^2 Q_{n+1}}{(\partial \boldsymbol{\sigma})^2} + (\delta\gamma_{n+1})^2 A \frac{\partial^2 Q_{n+1}}{\partial \boldsymbol{\sigma} \partial W^{cr}} \left[\frac{\partial^2 \tilde{Q}_{n+1}}{\partial W^{cr} \partial \boldsymbol{\sigma}} \right]^T, \\ \mathbf{D} &= \frac{\partial Q_{n+1}}{\partial \boldsymbol{\sigma}} + \delta\gamma_{n+1} A \frac{\partial^2 Q_{n+1}}{\partial \boldsymbol{\sigma} \partial W^{cr}} \frac{\partial \tilde{Q}_{n+1}}{\partial W^{cr}}. \end{aligned} \tag{47}$$

By differentiating the discrete consistency condition in Eq. (30) we get

$$\left[\frac{\partial F_{n+1}}{\partial \boldsymbol{\sigma}} \right]^T d\boldsymbol{\sigma}_{n+1} + \frac{\partial F_{n+1}}{\partial W^{cr}} dW_{n+1}^{cr} = 0. \tag{48}$$

1. Initialize: $\mathbf{\Delta u}_{n+1}^{cr(1)} = \mathbf{\Delta u}_n^{cr} \qquad W_{n+1}^{cr(1)} = W_n^{cr} \qquad \delta\gamma_{n+1}^{(1)} = 0$

2. Calculate actual stresses, fracture work, internal parameters and yield criterion:

IF $k = 1$ AND $b > 0$

IF $\Delta u_{N,n+1} - \Delta u_{N,n}^{pl} > 0$

$$\sigma_{N,n+1}^{(k)} = (1 - \omega_n)\, k_N(\Delta u_{N,n+1} - \Delta u_{N,n}^{pl})$$

ELSE

$$\sigma_{N,n+1}^{(k)} = k_N(\Delta u_{N,n+1} - \Delta u_{N,n}^{pl})$$

$$\sigma_{T1,n+1}^{(k)} = k_T(\Delta u_{T1,n+1} - \Delta u_{T1,n}^{cr})$$

$$\sigma_{T2,n+1}^{(k)} = k_T(\Delta u_{T2,n+1} - \Delta u_{T2,n}^{cr})$$

ELSE

$$\boldsymbol{\sigma}_{n+1}^{(k)} = \mathbf{C}\left[\mathbf{\Delta u}_{n+1} - \mathbf{\Delta u}_{n+1}^{cr(k)}\right]$$

$$\chi_{n+1}^{(k)} = \chi(\chi_0, W_{n+1}^{cr^{(k)}}) \qquad c_{n+1}^{(k)} = c(c_0, W_{n+1}^{cr^{(k)}})$$

$$F_{n+1}^{(k)} = F(\sigma_{n+1}^{(k)}, \chi_{n+1}^{(k)}, c_{n+1}^{(k)})$$

IF $\dfrac{F_{n+1}^{(k)}}{F_{\text{norm}}} < TOL$ AND $k = 1$ THEN GOTO 7.

$$\mathbf{R}_{n+1}^{\mathbf{\Delta u}^{cr}(k)} = \mathbf{\Delta u}_n^{cr} - \mathbf{\Delta u}_{n+1}^{cr^{(k)}} + \delta\gamma_{n+1}^{(k)} \frac{\partial Q_{n+1}^{(k)}}{\partial \boldsymbol{\sigma}}$$

$$R_{n+1}^{W^{cr}(k)} = W_n^{cr} - W_{n+1}^{cr(k)} + \delta\gamma_{n+1}^{(k)} \frac{\partial \tilde{Q}_{n+1}^{(k)}}{\partial W^{cr}}$$

IF $\sqrt{\left(\dfrac{F_{n+1}^{(k)}}{F_{\text{norm}}}\right)^2 + \left(\dfrac{||\mathbf{R}_{n+1}^{\mathbf{\Delta u}^{cr}(k)}||}{\Delta u_{\text{norm}}^{cr}}\right)^2 + \left(\dfrac{|R_{n+1}^{W^{cr}(k)}|}{W_{\text{norm}}}\right)^2} < TOL$ THEN GOTO 6.

3. Calculate increment of plastic multiplier:

$$\delta^2\gamma_{n+1}^{(k)} := \left[F_{n+1}^{(k)} - \left[\frac{\partial F_{n+1}^{(k)}}{\partial \mathbf{v}}\right]^T \mathbf{\Xi}_{n+1}^{(k)} \mathbf{R}_{n+1}^{(k)}\right] \left[\left[\frac{\partial F_{n+1}^{(k)}}{\partial \mathbf{v}}\right]^T \mathbf{\Xi}_{n+1}^{(k)} \frac{\partial Q_{n+1}^{(k)}}{\partial \mathbf{v}}\right]^{-1}$$

$$\mathbf{\Xi}_{n+1}^{(k)} = \begin{bmatrix} \mathbf{C}^{-1} + \delta\gamma_{n+1}^{(k)} \dfrac{\partial^2 Q_{n+1}^{(k)}}{(\partial \boldsymbol{\sigma})^2} & \delta\gamma_{n+1}^{(k)} \dfrac{\partial^2 Q_{n+1}^{(k)}}{\partial \boldsymbol{\sigma} \partial W^{cr}} \\ \delta\gamma_{n+1}^{(k)} \left[\dfrac{\partial^2 \tilde{Q}_{n+1}^{(k)}}{\partial W^{cr} \partial \boldsymbol{\sigma}}\right]^T & -1 + \delta\gamma_{n+1}^{(k)} \dfrac{\partial^2 \tilde{Q}_{n+1}^{(k)}}{(\partial W^{cr})^2} \end{bmatrix}^{-1}$$

$$\mathbf{R}_{n+1}^{(k)} = \begin{bmatrix} \mathbf{R}_{n+1}^{\mathbf{\Delta u}^{cr}(k)} \\ R_{n+1}^{W^{cr}(k)} \end{bmatrix}, \quad \frac{\partial Q_{n+1}^{(k)}}{\partial \mathbf{v}} = \begin{bmatrix} \dfrac{\partial Q_{n+1}^{(k)}}{\partial \boldsymbol{\sigma}} \\ \dfrac{\partial \tilde{Q}_{n+1}^{(k)}}{\partial W^{cr}} \end{bmatrix}, \quad \frac{\partial F_{n+1}^{(k)}}{\partial \mathbf{v}} = \begin{bmatrix} \dfrac{\partial F_{n+1}^{(k)}}{\partial \boldsymbol{\sigma}} \\ \dfrac{\partial F_{n+1}^{(k)}}{\partial W^{cr}} \end{bmatrix}$$

Table 1: General Closest Point Projection algorithm for the presented model (Part 1)

4. Calculate increments of inelastic relative displacements and of fracture work:

$$\begin{bmatrix} \delta\mathbf{\Delta u}_{n+1}^{cr(k)} \\ \delta W_{n+1}^{cr(k)} \end{bmatrix} = \begin{bmatrix} \mathbf{C}^{-1} & \mathbf{0} \\ \mathbf{0} & -1 \end{bmatrix} \mathbf{\Xi}_{n+1}^{(k)} \left[\mathbf{R}_{n+1}^{(k)} + \delta^2 \gamma_{n+1}^{(k)} \frac{\partial Q_{n+1}^{(k)}}{\partial \mathbf{v}} \right]$$

5. Actualize the iteration unknowns:

$$\mathbf{\Delta u}_{n+1}^{cr(k+1)} = \mathbf{\Delta u}_{n+1}^{cr(k)} + \delta\mathbf{\Delta u}_{n+1}^{cr(k)}$$

$$W_{n+1}^{cr(k+1)} = W_{n+1}^{cr(k)} + \delta W_{n+1}^{cr(k)}$$

$$\delta\gamma_{n+1}^{(k+1)} = \delta\gamma_{n+1}^{(k)} + \delta^2\gamma_{n+1}^{(k)}$$

SET $k = k + 1$ GOTO 2.

6. Update:

$$\mathbf{\Delta u}_{n+1}^{cr} = \mathbf{\Delta u}_{n+1}^{cr(k)}$$

$$W_{n+1}^{cr} = W_{n+1}^{cr(k)}$$

IF $b > 0$

IF $\sigma_{N,n+1}^{(k)} > 0$

$$f^D = f^D(\sigma_{N,n+1}^{(k)}, \sigma_{T1,n+1}^{(k)}, \sigma_{T2,n+1}^{(k)})$$

$$\Delta u_{N,n+1}^{pl} = \Delta u_{N,n}^{pl} + \left(\Delta u_{N,n+1}^{cr} - \Delta u_{N,n}^{cr}\right)\left(1 - bf^D\right)$$

$$\Delta u_{N,n+1}^{D} = \Delta u_{N,n+1}^{cr} - \Delta u_{N,n+1}^{pl}$$

$$\omega_{n+1} = \frac{\Delta u_{N,n+1}^{D}}{\Delta u_{N,n+1} - \Delta u_{N,n+1}^{pl}}$$

ELSE

$$\Delta u_{N,n+1}^{pl} = \Delta u_{N,n}^{pl} + \Delta u_{N,n+1}^{cr} - \Delta u_{N,n}^{cr}$$

$$\Delta u_{N,n+1}^{D} = 0$$

7. End

Normalization terms:

$$F_{\text{norm}} = \sqrt{c_0^2 + \chi_0^2 \tan^2\phi}$$

$$\Delta u_{\text{norm}}^{cr} = \min\left(\frac{2G_f^I}{\chi_0}, \frac{2G_f^{IIa}}{c_0}\right)$$

$$W_{\text{norm}}^{cr} = \min\left(G_f^I, G_f^{IIa}\right)$$

Table 2: General Closest Point Projection algorithm for the presented model (Part 2)

Substituting Eq. (44) in Eq. (48) yields

$$\mathbf{E}^T d\boldsymbol{\sigma}_{n+1} + G d\delta\gamma_{n+1} = 0, \tag{49}$$

with

$$\begin{aligned} \mathbf{E} &= \frac{\partial F_{n+1}}{\partial \boldsymbol{\sigma}} + \delta\gamma_{n+1} A \frac{\partial F_{n+1}}{\partial W^{cr}} \frac{\partial^2 \tilde{Q}_{n+1}}{\partial W^{cr} \partial \boldsymbol{\sigma}}, \\ G &= A \frac{\partial F_{n+1}}{\partial W^{cr}} \frac{\partial \tilde{Q}_{n+1}}{\partial W^{cr}}. \end{aligned} \tag{50}$$

Further substitution of Eq. (46) in Eq. (49) leads to the following equation

$$d\delta\gamma_{n+1} = H \mathbf{E}^T \mathbf{B}\, d\boldsymbol{\Delta}\mathbf{u}_{n+1}, \tag{51}$$

with

$$H^{-1} = \mathbf{E}^T \mathbf{B} \mathbf{D} - G. \tag{52}$$

Finally the algorithmic modulus is obtained by substituting Eq. (51) in Eq. (46) as follows

$$\begin{aligned} d\boldsymbol{\sigma}_{n+1} &= \mathbf{B} \left[d\boldsymbol{\Delta}\mathbf{u}_{n+1} - H \mathbf{D} \mathbf{E}^T \mathbf{B}\, d\boldsymbol{\Delta}\mathbf{u}_{n+1} \right] \\ \left. \frac{d\boldsymbol{\sigma}}{d\boldsymbol{\Delta}\mathbf{u}} \right|_{n+1} &= \mathbf{B} - H \mathbf{B} \mathbf{D} \mathbf{E}^T \mathbf{B}. \end{aligned} \tag{53}$$

3 NUMERICAL EXAMPLES

3.1 Verification of modified elasto-plastic model

This example is carried out according to [2] to verify the presented mixed-mode cohesive crack model for pure tension loading, for shear loading under constant compression and for combined loading assuming pure elasto-plastic behavior. The first two artificial tests have been designed in [2] and the material parameters are given in Table 4, where for the pure tension test only the Mode-I parameters are necessary, the Mode-II parameters can be chosen arbitrarily. In the third calculation the experimental results of the test in [7] are used for fitting the material parameters. The obtained parameters are given additionally in Table 4. During this test a prismatic concrete specimen of $7 \times 7cm$ cross section with a perimetral $1.5cm$ deep notch is subjected to pure tension, until the peak of normal stresses is reached and the tensile crack begins to form through the notched cross section. From this point on, normal and shear displacements are applied simultaneously in a fixed proportion characterized by $\tan\theta = \Delta u_N / \Delta u_T$.

The calculations are carried out here using a single interface element by performing a displacement controlled analysis. The mixed-mode CCM presented in this paper is investigated for all three tests with the modifications of the yield and potential surface as shown in Eq. (10) and Eq. (11). The results displayed in Fig. 7, 8 and 9 show excellent agreement with these obtained in [2]. The analytical solution for the pure tension problem is given in [2]. In Fig. 8 it can be seen, that the tangential stresses converge to the Coulomb friction values and that the dilatancy effect depends on the normal stress. Fig. 13 clarifies, that the model can represent the complex mixed-mode fracture process investigated in [7] very well.

3.2 Investigation of cyclic behavior

In this section we investigate the applicability of the presented model for cyclic loading. For this purpose first the pure tension test analyzed in the previous example is investigated

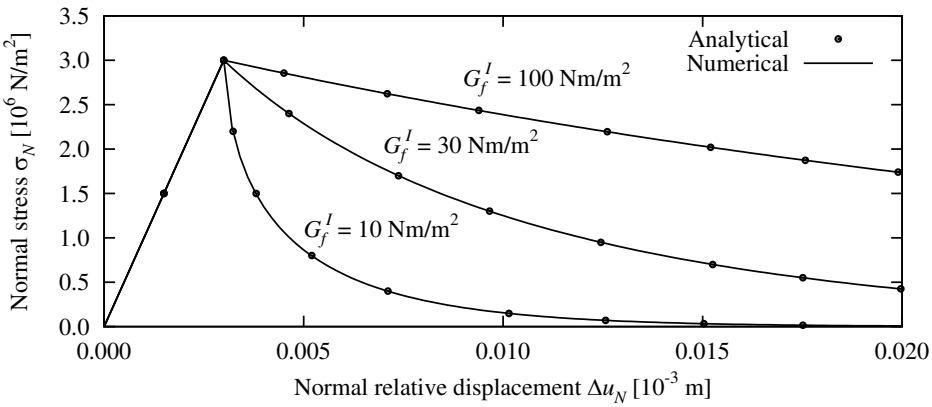

Figure 7: Pure tension: Normal stress vs. normal relative displacement for different values of Mode-I fracture energy

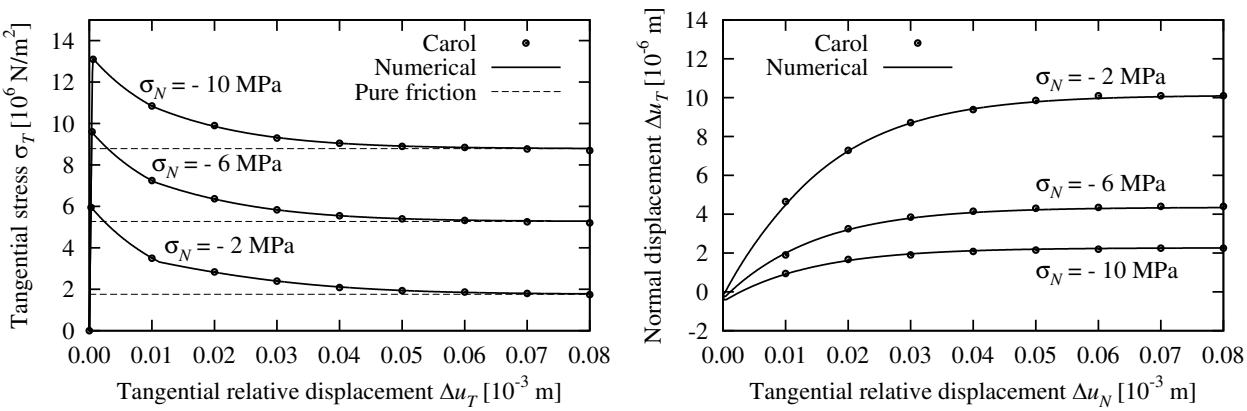

Figure 8: Shear under constant compression: Shear stress vs. tangential relative displacement and evolution of dilatancy for different values of compressive stress

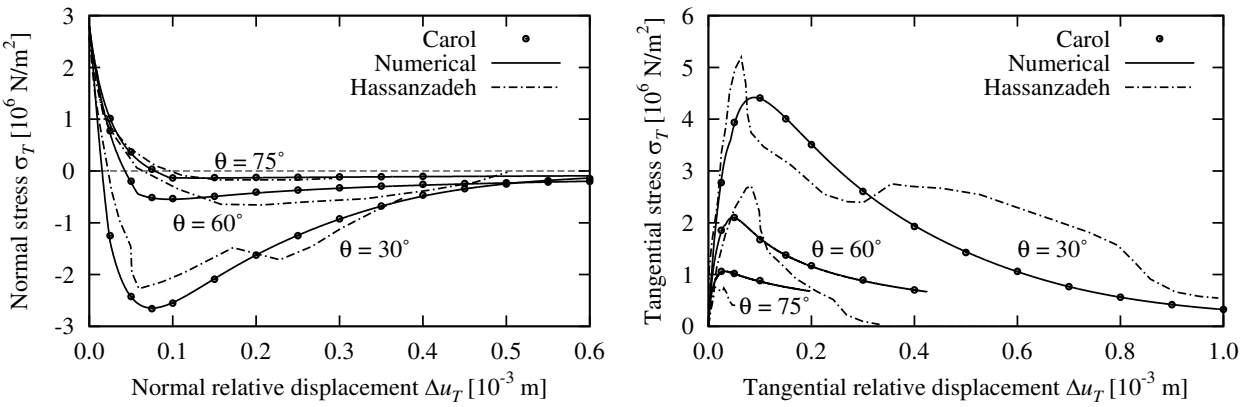

Figure 9: Hassanzadeh test: Normal stress vs. normal relative displacement and shear stress vs. tangential relative displacement

			Pure tension	Shear/compression	Hassanzadeh
Normal stiffness	k_N	$[10^9 N/m^3]$	1.0	25.0	200.0
Tangential stiffness	k_T	$[10^9 N/m^3]$	-	25.0	200.0
Tensile strength	χ_0	$[10^6 N/m^2]$	3.0	3.0	2.8
Shear strength	c_0	$[10^6 N/m^2]$	-	4.5	7.0
Mode-I fracture energy	G_f^I	$[Nm/m^2]$	$10, 30, 100$	30.0	100
Mode-IIa fracture energy	G_f^{IIa}	$[Nm/m^2]$	-	60.0	1000
Dilatancy stress	σ^{dil}	$[10^6 N/m^2]$	-	30.0	56.0
Friction coefficient	tan ϕ	[-]	-	0.8785	0.9
Shape parameter	α_χ	[-]	0.0	0.0	0.0
Shape parameter	α_c	[-]	-	0.0	-1.5
Shape parameter	α_σ^{dil}	[-]	-	-2.0	-2.7
Shape parameter	α_c^{dil}	[-]	-	0.0	3.0

Table 3: Parameters for verification of mixed-mode CCM according to (Carol et al. 1997)

for $G_f^I = 30Nm/m^2$. All other parameters are taken according to Table 4. Due to the pure tension loading the shape parameter α^D and the exponent γ of the damage scaling function f^D have no influence on the results. In Fig. 10 the calculated load displacement curves are shown for different values of the damage factor b defining the proportion between the plastic and the damage deformation rate. The figure indicates, that for $b = 0.0$ a pure plastic re- and unloading is obtained, whereby for $b = 1.0$ only damage deformations occur if $\sigma_N > 0$. For these cases as well as for the combined case with $b = 0.4$ the calculated results agree exactly with the analytical solution.

In the next analysis the shear test under constant normal stress is investigated using the plastic parameters in Table 4. First the influence of the damage factor b is analyzed for a normal stress of $\sigma_N = 10^5 Nm/m^2$. In Fig. 11 the obtained stress-displacement curves are shown, which agree exactly for all three values. This shows, that for monotonic loading, the calculated stresses agree always with the results from the elasto-plastic model, which is the major assumption in the extended model. Furthermore the influence of the shape parameter α^D and the exponent γ is investigated. In Fig. 11 their influence on the scalar damage value ω, which describes the actual damage state of the material, is shown. The figure indicates, that for $\gamma = 1$ the evolution of ω is almost independent of the normal stress σ_N due to the linear dependence of the damage deformations on the stresses and consequently on the elastic deformations. For $\gamma = 2$ the expected behavior, that with increasing normal stress compared to the tangential stress the damage evolution is accelerated, can be obtained as shown in Fig. 11. Additional Fig. 11 indicates that the modification of α^D can adapt the characteristics of the damage evolution very flexible.

4 IDENTIFICATION OF MODEL PARAMETERS USING NEURAL NETWORKS

In this section the model parameters are identified using a Multi-Layer-Perceptron neural network. The investigations are based on the algorithm presented in [8] where Latin Hypercube Sampling has been used to generate the training data sets. In the first step the pure tensile softening is analyzed. For this purpose the normal stress curve used as reference is obtained

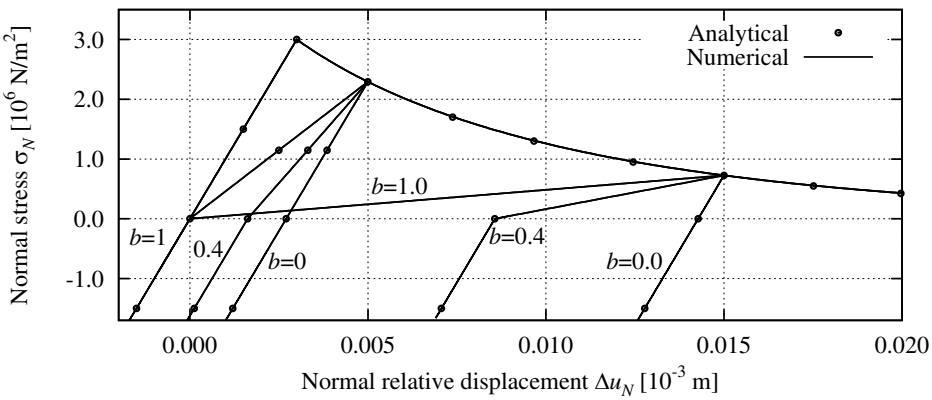

Figure 10: Pure tension: Normal stress vs. normal relative displacement for different values of damage factor

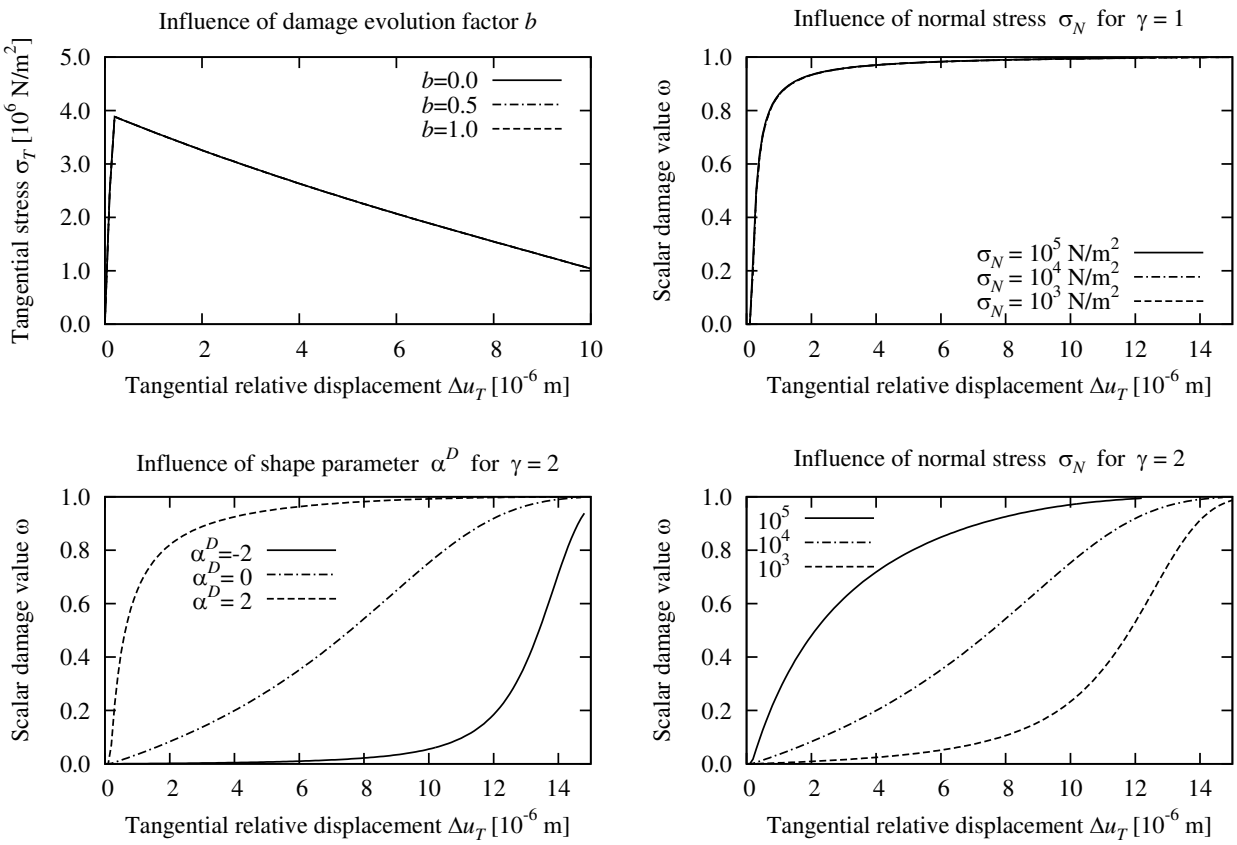

Figure 11: Shear under constant normal stress: Shear stress vs. tangential relative displacement ($\sigma_N = 10^5 Nm/m^2$, $\gamma = 1$ and $\alpha^D = 0$) and evolution of scalar damage value ω depending on the normal stress ($b = 1.0$ and $\alpha^D = 0$) for different exponents γ and on the shape parameter α^D ($\gamma = 2$, $b = 1.0$ and $\sigma_N = 10^4 Nm/m^2$)

with the following parameters: tensile strength $\chi_0 = 3 \cdot 10^6 N/m^2$, Mode-I fracture energy $G_f^I = 100 Nm/m^2$ and the shape parameter for tensile softening $\alpha_\chi = 0$. The corresponding softening curve depending on the inelastic crack displacements is shown in Fig. 12. All other parameters do not have an influence on the softening curve. Eleven regular points on this curve are used as input values and the three parameters as output values for the neural network approximation. In Fig. 12 the curve from the identified parameters using 100 uniformly distributed LHS training samples and 15 hidden neurons is shown additionally. This curve shows a very good agreement with the reference solution, which clarifies that the neural network approximation works very well for this problem.

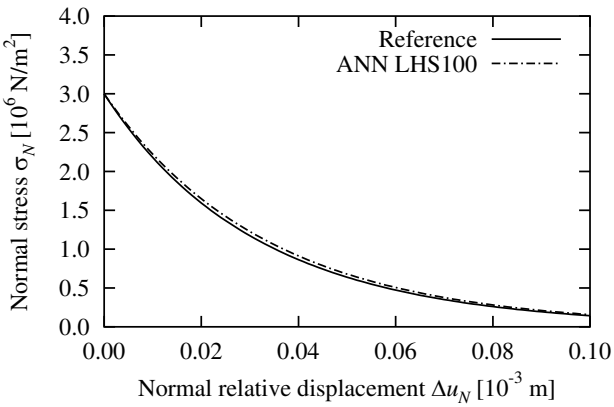

Figure 12: Tension softening curve from original and identified parameters

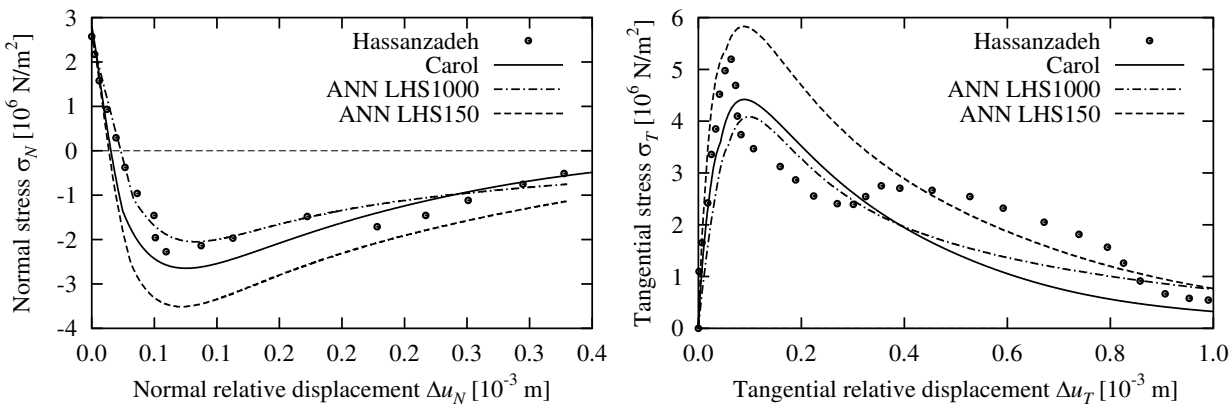

Figure 13: Normal and tangential stresses depending on the crack opening and sliding; Experimental and numerical curves with identified parameters

In the next step all twelve parameters of the elasto-plastic model are identified by means of a combined normal-shear-cracking test carried out by [7]. In Fig. 13 the measured curve for the normal and shear stress depending on the crack opening and sliding are shown. Additionally the curves obtained from the parameters identified by [2] using an optimization strategy are displayed. The parameters are given in Table 4. The neural network approximation is carried out using 150 uniformly distributed LHS samples with 4 hidden neurons and 1000 LHS samples with 29 hidden neurons. The training bounds and the identified parameters using 10 points from each curve are given in Table 4. Fig. 13 shows the curves belonging to these parameters. With 150 training samples the estimated parameters do not lead to a sufficient agreement of

the normal and tangential stresses. If 1000 samples are used the agreement is much better and the resulting curves close to these obtained by [2]. But a very good agreement with the experimental curves is not achieved, which might be caused on the one hand by the ill-conditioned experimental curve with softening and hardening, which can not represented by the material model. On the other hand the complexity of the problem, which needs much more neurons for a very good representation, might by another reason. With 4 neurons the minimum mean square error of the training is about 0.23 and with 29 neurons about 0.13, which shows that the training fitting improves with increasing number of samples and neurons, but for a very good fitting with a mean square error for example below 10^{-5} a much larger number of neurons and belonging training samples might be necessary. Although the neural network approximation leads to similar results as the application of classical optimization strategies.

			Carol	Training	ANN LHS150	ANN LHS1000
Normal stiffness	k_N	$[10^9 N/m^3]$	200	$100-500$	314	155
Tangential stiffness	k_T	$[10^9 N/m^3]$	200	$100-500$	301	102
Tensile strength	χ_0	$[10^6 N/m^2]$	2.8	$2.0-3.5$	2.5	2.6
Shear strength	c_0	$[10^6 N/m^2]$	7.0	$4.0-10.0$	8.0	9.9
Mode-I fract. energy	G_f^I	$[Nm/m^2]$	100	$50-300$	156	105
Mode-IIa fract. energy	G_f^{IIa}	$[Nm/m^2]$	1000	$500-2000$	1670	1590
Dilatancy stress	σ^{dil}	$[10^6 N/m^2]$	56	$20-100$	65	76
Friction coefficient	tan ϕ	[-]	0.9	$0.5-1.0$	0.83	0.87
Shape parameter	α_χ	[-]	0.0	$-1.0-1.0$	-0.04	-0.11
Shape parameter	α_c	[-]	-1.5	$-3.0-0.0$	-1.33	-2.16
Shape parameter	α_σ^{dil}	[-]	-2.7	$-6.0-0.0$	-2.53	-3.57
Shape parameter	α_c^{dil}	[-]	3.0	$0.0-6.0$	2.91	3.29

Table 4: Identified parameters and training bounds

5 CONCLUSIONS

In this paper a cohesive crack model for combined crack opening and sliding presented by [2] has been extended for cases with un- and reloading using a combined plastic-damage formulation which enables the modeling of crack opening and crack closure. By means of several numerical examples the model has been verified for the elasto-plastic state according to [2]. For the numerical examples investigating the damage behavior of the model a simple tension test and a shear test under constant normal stress have been chosen. It could be shown, that the numerical implementation can represent the assumption of the material model, such as the given proportion between damage and plastic deformations and the acceleration of the damage evolution due to an increasing normal stress compared to the tangential stress, and that the introduced parameters enable a flexible adaptation of the damage characteristics. For further investigations the verification by means of experimental results with cycling loading would be interesting.

Finally an investigation concerning the identification of the model parameters by means of neural networks was presented. It could be shown, that the elasto-plastic model parameters could be identified well with this approach, but require a huge number of simulations. In a

further study the numerical effort of the parameter identification for this model using neural networks is compared to the effort by means of classical optimization strategies.

ACKNOWLEDGEMENT

This research has been supported by the German Research Council (DFG) through Collaborative Research Center 524, which is gratefully acknowledged by the authors.

REFERENCES

[1] M. Hillerborg, M. Modeer, and P. E. Peterson. Analysis of crack formation and crack growth in concrete by means of fracture mechanics and finite elements. *Cement and Concrete Research*, 6:773–782, 1976.

[2] I. Carol, P. C. Prat, and C. M. López. Normal/shear cracking model: Application to discrete crack analysis. *Journal of Engineering Mechanics ASCE*, 123:765–773, 1997.

[3] K. Schrader. Algorithmische Umsetzung eines elasto-plastischen Kontakt-Materialgesetzes zur Abbildung der Rissflächen-Degradation bei kohäsiven Rissen. Diploma thesis, Bauhaus-University Weimar, Germany, 2005.

[4] T. Most. *Stochastic crack growth simulation in reinforced concrete structures by means of coupled finite element and meshless methods*. PhD thesis, Bauhaus-University Weimar, Germany, 2005.

[5] T. Most and C. Bucher. Energy-based simulation of concrete cracking using an improved mixed-mode cohesive crack model within a meshless discretization. *International Journal for Numerical and Analytical Methods in Geomechanics, accepted for publication*, 2006.

[6] J. R. Simo and T. J. R. Hughes. *Computational Inelasticity*. Springer, New York, 1998.

[7] M. Hassanzadeh. Determination of fracture zone properties in mixed mode I and mode II. *Engineering Fracture Mechanics*, 35:845–853, 1990.

[8] D. Lehký and D. Novák. Identification of material model parameters using stochastic training of neural network. In Walraven et al., editors, *Proc. 5th Int. PhD Symposium in Civil Engineering, Delft, Netherlands, June 16-19, 2004*. Balkema, Rotterdam, 2004.